Structure and phase behavior of polyelectrolyte star solutions

Norman Hoffmann, Christos N. Likos, and Hartmut Löwen

Citation: The Journal of Chemical Physics **121**, 7009 (2004); doi: 10.1063/1.1790451
View online: https://doi.org/10.1063/1.1790451
View Table of Contents: http://aip.scitation.org/toc/jcp/121/14
Published by the American Institute of Physics

Structure and phase behavior of polyelectrolyte star solutions

Norman Hoffmann, Christos N. Likos, and Hartmut Löwen
Institut für Theoretische Physik II, Heinrich-Heine-Universität Düsseldorf, Universitätsstraße 1, Düsseldorf D-40225, Germany

(Received 8 March 2004; accepted 15 July 2004)

Using the recently developed effective interaction potentials between polyelectrolyte stars, we examine the structure and phase behavior of solutions of the same. The effective interaction is ultrasoft and density dependent, owing to the integration of the counterionic degrees of freedom. The latter contribute extensive volume terms that must be taken into account in drawing the phase diagram of the system. The structural behavior of the uniform fluid is characterized by anomalous structure factors, akin to those found previously for solutions of uncharged star polymers. The phase diagram of the system is very rich, featuring a fluid phase at low arm numbers of the stars, two reentrant melting regions, as well as a variety of crystal structures with unusual symmetry. The physical origin of these features can be traced back to the ultrasoft nature of the effective interaction potential. © *2004 American Institute of Physics.* [DOI: 10.1063/1.1790451]

I. INTRODUCTION

The two most commonly used mechanisms for stabilizing colloidal suspensions against flocculation caused by the dipole-dipole dispersion forces are charge stabilization and steric stabilization. In the former case, the charge on the colloidal particles is responsible for an electrostatic repulsion (screened by the counterions in the solution) which suppresses the dispersion attraction. In the latter case, polymer chains grafted or adsorbed on the surface of the colloids provide a repulsive barrier against coagulation due to their mutual excluded-volume interactions. The two stabilization mechanisms can be combined by grafting charged polymer chains or *polyelectrolytes* (PEs) on the colloids and in this way spherical polyelectrolyte brushes are formed. Spherical PE brushes are flexible systems which can assume a large number of different conformations, depending on the values of the physical parameters of the system. When the size of the colloidal particle, R_c, is much larger than the brush height L, one speaks of *crew-cut brushes*, whereas in the opposite limit, $R_c \ll L$, one obtains *polyelectrolyte stars*. Experimentally, PE brushes can be realized either by physically grafting PEs on a hard colloid or by using block copolymers with one hydrophobic neutral block and one charged block. In this case, charged block copolymer micelles result, which closely resemble PE brushes.

In dealing with spherical PE brushes or stars, one distinguishes between weak or *annealed* ones and strong or *quenched* ones.[1] In the former case, the ionization constant of the monomers is low, hence the actual charge on the brush depends on the local electrostatic conditions, due to the possibility of charge recombination. In the latter case, the ionization constant is high and hence the charge on the brushes is constant, irrespective of the details of the system. A considerable number of studies have been dedicated to the analysis of the sizes and conformations of spherical PE brushes and stars, since the number of physical parameters to be tuned (chain length, degree of ionization, pH and salinity of the solution, solvent quality, temperature) is large and a corresponding flexibility in the possible conformation results. Pincus was the first to assume that quenched PE stars with a high charging fraction would be characterized by strongly stretched chains and an absorption of the majority of the dissolved counterions.[2] Klein Wolterink *et al.*[1,3] as well as Borisov and Zhulina[4,5] applied scaling theory and self-consistent field (SCF) calculations to study the conformations of PE stars. One important finding of these works is the stretching of the chains and the absorption of counterions for strongly charged, quenched chains. PE stars falling in this regime are called *osmotic*.[6] The rodlike character of the chains in osmotic PE stars was also confirmed in extensive molecular dynamics (MD) simulations of Jusufi *et al.*[7,8] and in the Monte Carlo (MC) simulations of Roger *et al.*[9] Recently, Borisov and Zhulina have also put forward mean-field calculations for block copolymer micelles with one neutral and one charged block, which self-assemble in solution.[10–12] There, emphasis was put on the effect of salt on the *morphological* transitions from crew-cut to starlike micelles and even on the geometrical transformations between micelles, cylinders, and lamellae. However, in this work we consider PE stars for which the chains are chemically anchored on a small solid core particle, hence the architecture is fixed and morphological transitions can be ruled out.

From the experimental point of view, the stretching of the chains in osmotic PE brushes has been confirmed in small-angle neutron scattering experiments (SANS) of Guenoun *et al.*[13] A comprehensive SANS study of spherical micelles with a charged corona was carried out by van der Maarel co-workers.[14–16] It was demonstrated that the counterions remain confined mainly within the corona and that the charged chains assume a rodlike configuration. Dynamic light scattering (DLS) studies of the corona size for both quenched and annealed PE brushes were carried out by Guo and Ballauff,[17] who found that with increasing pH annealed brushes exhibit a transition to fully stretched chains. Finally, recent anomalous small-angle x-ray scattering experiments

(ASAXS) by Dingenouts *et al.*[18] have demonstrated that the density profile of the trapped counterions follows that of the charged monomers along the chains, in agreement with predictions from theory and simulations.[7,8]

Although the conformational regimes of PE stars and brushes have thus been studied to a considerable extent, very little is known about the correlations between PE stars in concentrated solutions and about the phase behavior of the latter. In their recent SAXS experiments from salt-free solutions of star-branched polyelectrolytes, Heinrich *et al.* found an anomalous behavior of the position of the main peak of the interstar structure factor.[19] In particular, although below the overlap concentration its position scales with the one-third power of the concentration, it shows a much weaker dependence on the density thereafter. In order to understand theoretically the features of the interstar correlations, a coarse-graining approach is necessary, in which the chains and the counterions are traced out, leaving behind only the star centers as relevant degrees of freedom. These interact by means of an effective potential that has its physical origin on the integrated-out degrees of freedom.[20] This coarse-graining approach was carried out recently by Jusufi *et al.*,[7,8] bridging the gap from the microscopic to the mesoscopic description of the system. The purpose of this work is to carry now the next step in the bridging of the length scales and go from the mesoscopic to the macroscopic scale. In particular, by employing the effective interactions derived in Ref. 8, we study systematically the nature of the pair correlations and we determine the thermodynamics of the fluid state. By comparing with the free energies of many candidate crystalline phases, we then draw the phase diagram of the system and find a host of unusual crystal structures and a rich topology of the phases.

The rest of the paper is organized as follows: In Sec. II, we first briefly review the derivation of the effective pair potential for the two-body problem, generalizing it afterwards to the many-body system and deriving the Hamiltonian that includes an extensive, coordinate-independent volume term. In Sec. III we apply standard tools from liquid-state theory to derive the structure and thermodynamics of the fluid state, whereas a harmonic theory is applied in Sec. IV in order to calculate the free energies of various crystalline phases. On this basis, the phase diagram of the system is drawn and discussed in Sec. V. Finally, in Sec. VI we summarize and conclude. Some technical considerations regarding the compressibility of the system are presented in the Appendix.

II. THE EFFECTIVE HAMILTONIAN

In this section, we briefly review the theoretical model that has led on the one hand to the determination of the properties of isolated PE stars and on the other hand to the derivation of an effective interaction potential $V_{\mathrm{eff}}(D)$ between the star centers, where D denotes their mutual separation. As far as the derivation of the effective potential is concerned, we limit ourselves to an outline and refer the reader to Refs. 7, 8, and 21 for details. We then employ the pair potential approximation in order to write down the effective Hamiltonian of the many-body system, taking into consideration the extensive terms that arise from integrating out the microscopic degrees of freedom of the system.

A. Determination of the pair interaction potential

We consider PE stars at room temperature T, dissolved in an aqueous solvent. Here we consider exclusively the salt-free case but the procedure for deriving effective interactions in the presence of salt has also been worked out and can be found in Ref. 8. Let N_s be the number of PE stars dissolved in the macroscopic volume Ω occupied by the system and $\rho_s=N_s/\Omega$ their density. Every chain of the PE star consists of N monomers and is charged in a periodical manner with charging fraction α, i.e., every $1/\alpha$th monomer along the chains bears the elementary charge e. The Bjerrum length $\lambda_B=e^2/(\epsilon k_B T)$ has the value 7.1 Å, taking $\epsilon=81$ as the dielectric constant of water, where k_B denotes the Boltzmann constant. All PE stars have the same functionality f and every chain carries N monomers. As a result, every star carries a charge $Q=efN\alpha$, leaving behind $N_c=\alpha fN$ monovalent counterions in the mixture. Every star is envisioned as sphere of radius R, surrounded by the Wigner-Seitz sphere of radius R_W. The latter is determined by the density ρ_s of the solution through the relation $\rho_s=3/(4\pi R_W^3)$. The counterions can therefore be found anywhere in the sphere of radius R_W and are further partitioned into three different states: N_1 *cylindrically condensed* counterions are confined to move in narrow cylinders around the branches of the star; N_2 *spherically trapped* counterions can explore the whole interior of the star with exception of the region for the condensed counterions; and, finally, N_3 counterions can move freely in the bulk of the solution and are located at $R<r<R_W$ in the model. We refer to the latter as *free* counterions. Clearly, $N_1+N_2+N_3=\alpha fN$. The numbers of counterions in every state as well as the star radius R have been determined variationally within a free energy function $\tilde{f}(R,\{N_i\})$, $i=1,2,3$, that includes electrostatic, steric as well as entropic contributions from the counterions.[7,8] Introduction of the minimizing values of these parameters back into the variational free energy allows then for the determination of the free energy f_1 of an isolated PE star. Since the counterion distributions vary with the system density, due to the dependence of the free energy on R_W, f_1 becomes a function of the concentration, $f_1=f_1(\rho_s)$. The presence of this term in the total free energy of an interacting PE star system is very important for the the phase behavior of the same, since it gives rise to the so-called *volume term* of the solution. Thereby, the specific form of the functional dependence of f_1 on ρ_s plays a crucial role in influencing the convexity of the free energy and the associated possibility of spontaneous fluid–fluid phase separation with a large density gap. We will return to this point in Sec. II C below.

We define the overlap density ρ_s^* through the condition $(\pi/6)\rho_s^*\sigma^3=1$, with $\sigma=2R$ denoting the diameter of the PE stars, yielding the value $\rho_s^*\sigma^3=1.91$. The effective interaction potential $V_{\mathrm{eff}}(D)$ has been determined by extending the cell model to two interacting stars and taking into account the fact that, upon close approaches, the chains of each star remain stretched but those belonging to different stars do not

interdigitate.[7,8] The approach yields the constrained Helmholtz free energy $\mathcal{F}_2(D)$ of the two interacting stars whose centers are kept at separation D, and which includes *all* contributions from the monomers and the counterions. In order to explicitly fulfill the requirement that the effective interaction vanish at infinite distances, $V_{\rm eff}(D)$ has been defined as[8]

$$V_{\rm eff}(D;\rho_{\rm s}) = \mathcal{F}_2(D;\rho_{\rm s}) - \mathcal{F}_2(D\to\infty;\rho_{\rm s}) = \mathcal{F}_2(D;\rho_{\rm s}) - 2\,f_1(\rho_{\rm s}). \quad (1)$$

The second line in Eq. (1) above follows from the fact that the total free energy of two stars infinitely far apart from one another is simply twice the free energy of an isolated star. Important for what follows is the *explicit* density dependence of the interaction potential on the density of the solution, which stems from the process of carrying out a partial trace over the microscopic degrees of freedom. Special care has to be taken whenever effective interaction potentials with explicit dependence on thermodynamic quantities, such as density or temperature, are employed,[22–25] therefore we need to elaborate on the physical origin of this dependence.

Below the overlap density, $\rho_{\rm s}<\rho_{\rm s}^*$, there is space for the counterions to move free in the solution. Hence, only a density dependent fraction of those is trapped (cylindrically or spherically) within the stars, with the effect that the latter carry a net charge. Consequently, for interstar distances $D>\sigma$, one obtains an interaction between charged spherical colloids, screened by the free counterions, that has the form of a Yukawa potential: $V_{\rm eff}^{>}(D)\sim\exp(-\kappa r)/r$, where the superscript denotes the condition $D>\sigma$. We emphasize here that the cell model is employed in order to determine the counterion distribution inside and outside the interacting stars, as well as the effective interaction for distances $D<\sigma$. For $D>\sigma$ the interaction is *assumed* to be of a Yukawa-type and it is *not* derived in the framework of the cell model. The constant κ is the well-known inverse Debye screening length, given by[21]

$$\kappa = \sqrt{\frac{3N_3\lambda_{\rm B}}{R_{\rm W}^3-R^3}}, \quad (2)$$

where it has been taken into account that *only* the N_3 free counterions per star screen the electrostatic interaction. The density dependence of the branch $V_{\rm eff}^{>}(D;\rho_{\rm s})$ of the effective potential comes, on the one hand, from the explicit $R_{\rm W}$ dependence of κ in Eq. (2) above and, on the other, from the dependence of the number of free counterions N_3 on the same quantity. The quantity N_3 rapidly approaches zero as $\rho_{\rm s}\to\rho_{\rm s}^*$ but otherwise it has a rather weak $\rho_{\rm s}$ dependence for a broad region of $\rho_{\rm s}<\rho_{\rm s}^*$. The branch $V_{\rm eff}^{<}(D;\rho_{\rm s})$, valid for $D<\sigma$, contains electrostatic, steric as well as entropic contributions arising mainly from the N_2 spherically trapped counterions of every star. All these quantities vary with the density $\rho_{\rm s}$ of the solution and $V_{\rm eff}^{<}(D;\rho_{\rm s})$ picks up a concomitant $\rho_{\rm s}$ dependence. The two branches of the effective potential, $V_{\rm eff}^{<}(D;\rho_{\rm s})$ and $V_{\rm eff}^{>}(D;\rho_{\rm s})$ are matched at $D=\sigma$ under the condition that the interaction and its derivative with respect to D be continuous there. For more details in the matching procedure we refer the reader to Refs. 8 and 21.

Above the overlap density, $\rho_{\rm s}>\rho_{\rm s}^*$, things are simpler. All counterions are now absorbed within the stars, which are therefore electroneutral. Thus, for $D>\sigma$, the effective interaction potential vanishes identically, $V_{\rm eff}^{>}(D)=0$. For $D<\sigma$, the interaction is governed by the entropic contributions of the trapped counterions. However, their number does not any more vary with density: there is no free space in the solution so that the counterions can partition themselves into free and trapped, thus there is no dependence of $V_{\rm eff}^{<}(D)$ on the concentration. Moreover, the procedure for deriving $V_{\rm eff}^{<}(D)$ yields in this case a function that smoothly approaches zero at $D=\sigma$, so that the $V_{\rm eff}^{<}(D)$ branch matches with the identically vanishing $V_{\rm eff}^{>}(D)$ branch automatically.[8] To be explicit, $V_{\rm eff}^{<}(D)$ for $\rho_{\rm s}>\rho_{\rm s}^*$ is given by the expression

$$\beta V_{\rm eff}^{<}(D) = N_2(D)\ln\left(\frac{N_2(D)}{4\pi\left\{1+\frac{D}{\sigma}\left[1-\ln\left(\frac{D}{\sigma}\right)\right]\right\}}\right) + \frac{N_2(D)}{1+\frac{D}{\sigma}\left[1-\ln\left(\frac{D}{\sigma}\right)\right]}\frac{D}{\sigma}\ln^2\left(\frac{D}{\sigma}\right) + N_2(D) - 2N_2^{(1)}\left[\ln\left(\frac{N_2^{(1)}}{4\pi}\right)+1\right], \quad (3)$$

where $N_2(D)$ is the number of spherically trapped counterions for two PE stars at distance D and $N_2^{(1)}$ is the same quantity for a single PE star. The expression for the quantity $N_2(D)$, which is the number of spherically trapped counterions for two stars at a distance D, is given in Eq. (37) of Ref. 8, whereas $N_2^{(1)}$ is given by Eqs. (22) and (23) in the same citation.

Summarizing, we are dealing with an effective interaction $V(D;\rho_{\rm s})$ that features a dependence on the density $\rho_{\rm s}$ below the overlap concentration and it is free of any density dependence above the overlap concentration. Quantitatively, this interaction is *ultrasoft* and *bounded*, i.e., it grows slower than any inverse-power law as $D\to 0$ and remains finite at $D=0$. The latter property is associated with the fact that we ignore the direct interaction between the centers of the stars, which is of microscopic range and has no effect on the structure and phase behavior of the macroscopic system. It is rather the chain- and counterion-mediated effective potential $V_{\rm eff}$, whose range is mesoscopic, that determines the behavior of the solution, which will be presented in the following sections. In Fig. 1, we show the effective potential for PE stars for two different combinations of functionalities f and charging fractions α, both below and above the overlap density. In this figure and all others that follow, the results pertain to a degree of chain polymerization $N=50$. It can be seen that with increasing $\rho_{\rm s}$ the interaction becomes softer, until one reaches $\rho_{\rm s}^*$, at which point the density dependence drops out. Moreover, for a given density, $V_{\rm eff}$ becomes more repulsive as f and/or α grows.

B. The many-body system

Interaction potentials that feature an explicit density dependence have to be treated with special consideration.

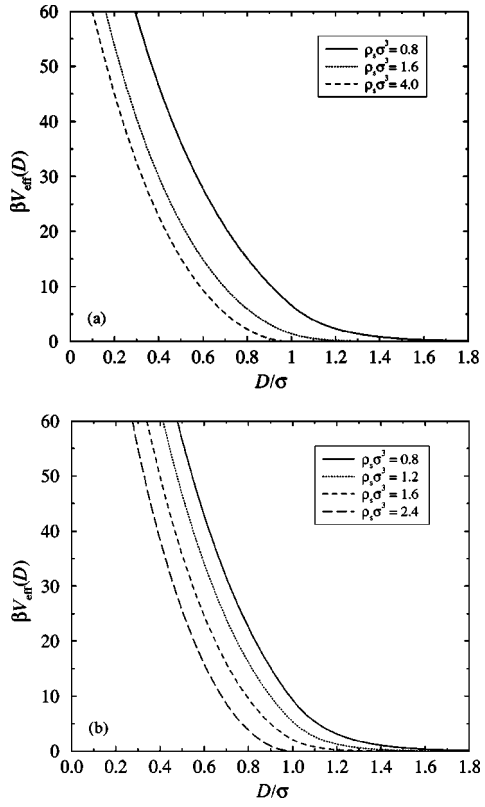

FIG. 1. The effective interaction potential for PE stars as a function of the star concentration ρ_s for two different combinations of the functionality f and the charge fraction α. (a) $f=10$, $\alpha=1/4$; (b) $f=15$, $\alpha=1/3$.

Strictly speaking, a *true* Hamiltonian function should involve solely the canonical coordinates of the degrees of freedom that characterize the system, i.e., the positions and momenta of the fundamental statistical units constituting the mixture. In a microscopic description, where all monomers, counterions, and solvent molecules are considered explicitly, this is indeed the case. Once, however, some microscopic degrees of freedom are traced out and one switches over to a mesoscopic, coarse-grained view of the complex fluid, explicit dependencies of the effective interaction on thermodynamic quantities cannot be ruled out. The effective potential loses then the rigorous meaning it has in a microscopic scale. As it has been pointed out recently in the literature, in such cases the effective interaction can only be used in the context in which it has been derived.[22,26] Certain sum rules or paths to the thermodynamics of the system, such as the compressibility or virial routes, which are valid and equivalent to one another for simple fluids, do not necessarily maintain their validity for density dependent effective potentials.[22,23,25] In fact, they not even *need* to be equivalent to each other. If, for example, the effective potential has been derived under the procedure of fitting simulation data for the compressibility of the system, then it is allowed to calculate the free energy of the complex fluid via the compressibility route but employing the virial route for the same effective potential will yield results that are neither consistent with the compressibility one nor valid altogether.[22] Therefore, it is crucial to specify the context in which the effective potential $V_{\mathrm{eff}}(D;\rho_s)$ of this work has been derived.

Our starting point is Eq. (1). First, consider a solution containing only two PE stars and let Q_2 be the canonical partition function of the system. The coordinates of the centers of the two stars are given by $\mathbf{R}_i$ and their momenta by $\mathbf{P}_i$, $i=1,2$. Clearly, $D=|\mathbf{R}_1-\mathbf{R}_2|$. The free energy of the two-star system is $F_2=-k_BT\ln Q_2$. The quantity $\mathcal{F}_2(D)$ in Eq. (1) is simply the constrained free energy $-k_BT\ln\mathcal{Q}_2(\mathbf{R}_1,\mathbf{R}_2)$ of the system,[20] when the first star is held fixed at position $\mathbf{R}_1$ and the second at position $\mathbf{R}_2$. The constrained partition function $\mathcal{Q}_2(\mathbf{R}_1,\mathbf{R}_2)$ is obtained by tracing out canonically all other particles while keeping the star centers fixed. The full partition function Q_2 is then calculated by taking the integral of its constrained counterpart $\mathcal{Q}_2(\mathbf{R}_1,\mathbf{R}_2)$ over all position vectors $\mathbf{R}_1$, $\mathbf{R}_2$ and, in addition, tracing out canonically the momenta of the two particles, in order to take into account their kinetic energies once the constraint of holding them fixed has been lifted. Specifically we have,[20]

$$Q_2=\frac{h^{-6}}{2!}\Omega^2\int\int\prod_{i=1}^{2}d^3P_i\exp\left(-\frac{\beta\mathbf{P}_i^2}{2m}\right)\times\frac{1}{\Omega^2}\int d^3R_1\int d^3R_2\,\exp[-\beta V_{\mathrm{eff}}(|\mathbf{R}_1-\mathbf{R}_2|;\rho_s)]\times\exp[-2\beta f_1(\rho_s)]. \tag{4}$$

In Eq. (4) above, h denotes Planck's constant, $\beta=(k_BT)^{-1}$, and m is the mass of the central particle.

We now generalize these considerations to a solution containing N_s PE stars, making further the physical assumption of *pair additivity* of the interactions. In other words, we fix the centers of the PE stars at the positions $\mathbf{R}_1,\mathbf{R}_2,\ldots,\mathbf{R}_{N_s}$ (collectively $\{\mathbf{R}\}$) and we assume that the corresponding constrained free energy $\mathcal{F}_{N_s}(\{\mathbf{R}\})$ is given, in analogy to Eq. (1), by the expression

$$\mathcal{F}_{N_s}(\{\mathbf{R}\})=\frac{1}{2}\sum_{i\neq j}^{N_s}V_{\mathrm{eff}}(|\mathbf{R}_i-\mathbf{R}_j|;\rho_s)+N_sf_1(\rho_s). \tag{5}$$

The total partition function Q_{N_s} is obtained as the generalization of Eq. (4) by the relation

$$Q_{N_s}=\frac{h^{-3N_s}}{N_s!}\Omega^{N_s}\int d\mathbf{P}^{N_s}\prod_{i=1}^{N_s}\exp\left(-\frac{\beta\mathbf{P}_i^2}{2m}\right)\times\frac{1}{\Omega^{N_s}}\int d\mathbf{R}^{N_s}\exp\left[-\frac{\beta}{2}\sum_{i\neq j}^{N_s}V_{\mathrm{eff}}(|\mathbf{R}_i-\mathbf{R}_j|;\rho_s)\right]\times\exp[-N_s\beta f_1(\rho_s)], \tag{6}$$

where $\int d\mathbf{P}^{N_s}$ is a shorthand for the multiple integral $\int\int\cdots\int d^3P_1d^3P_2\cdots d^3P_{N_s}$, and similarly for the position coordinates. Let Z_{N_s} denote the second factor on the right-hand side of Eq. (6) above. The total Helmholtz free energy of the system, F_{N_s} is given as $-k_BT\ln Q_{N_s}$ and Eq. (6) yields

$$F_{N_s}=F_{\mathrm{id}}+F_{\mathrm{ex}}+F_{\mathrm{vol}}=k_BTN_s[\ln(\rho_s\Lambda^3)-1]-k_BT\ln Z_{N_s}+N_sf_1(\rho_s), \tag{7}$$

where $\Lambda=\sqrt{\beta h^2/(2\pi m)}$ is the thermal de Broglie wavelength. The free energy is thus composed of the ideal part F_{id} stemming from the kinetic contributions, the excess part F_{ex} caused by the interactions *and* an extensive contribution $F_{\mathrm{vol}}=N_{\mathrm{s}}f_1(\rho_{\mathrm{s}})$ that constitutes the *volume term* of the free energy.[27] Though the latter has no effect on the interstar correlation functions, it does affect the values of thermodynamic quantities. Hence, the process of integrating out the microscopic degrees of freedom not only brings about a density dependence of the effective interactions but produces residual terms in the free energy as well, which cannot be ignored if one is interested in the full thermodynamics of the system.

We can now define the effective Hamiltonian $\mathcal{H}_{\mathrm{eff}}$ for the many-body PE-star solution as

$$\mathcal{H}_{\mathrm{eff}}=\sum_{i=1}^{N_{\mathrm{s}}}\frac{\mathbf{P}_i^2}{2m}+\frac{1}{2}\sum_{i\neq j}^{N_{\mathrm{s}}}V_{\mathrm{eff}}(|\mathbf{R}_i-\mathbf{R}_j|;\rho_{\mathrm{s}})+N_{\mathrm{s}}f_1(\rho_{\mathrm{s}}). \quad (8)$$

According to Eqs. (5)–(7) above, this Hamiltonian fulfills by its construction the condition of conservation of the total free energy of the assembly, which can be expressed as

$$F_{N_{\mathrm{s}}}=-k_{\mathrm{B}}T\ln\left[\frac{h^{-3N_{\mathrm{s}}}}{N_{\mathrm{s}}!}\int d\mathbf{P}^{N_{\mathrm{s}}}\int d\mathbf{R}^{N_{\mathrm{s}}}\exp(-\beta\mathcal{H}_{\mathrm{eff}})\right]. \quad (9)$$

There exist no ambiguities regarding the calculation of thermodynamic quantities, such as compressibility, pressure, internal energy, and so on. Eqs. (8) and (9) are to be considered together, i.e., our effective Hamiltonian is valid in the context of Eq. (9): it allows for the calculation of the total free energy of the system, from which then all relevant thermodynamic quantities can be derived in a standard way. Equation (9) is the key expression for the determination of the correlation functions between the star centers and for the subsequent derivation of the excess free energy F_{ex} in the fluid state, as will be discussed in Sec. III.

C. The volume term

The stability of uniform phases with respect to a spontaneous separation into a dilute and a dense configuration is determined by the convexity of the fluid free energy density $f_{\mathrm{fl}}(\rho_{\mathrm{s}})\equiv F_{N_{\mathrm{s}}}/\Omega$ with respect to ρ_{s}. Defining also $f_{\mathrm{ex}}\equiv F_{\mathrm{ex}}/\Omega$, Eq. (7) yields

$$f_{\mathrm{fl}}(\rho_{\mathrm{s}})=k_{\mathrm{B}}T\rho_{\mathrm{s}}[\ln(\rho_{\mathrm{s}}\sigma^3)-1]+f_{\mathrm{ex}}(\rho_{\mathrm{s}})+f_{\mathrm{vol}}(\rho_{\mathrm{s}})+3k_{\mathrm{B}}T\rho_{\mathrm{s}}\ln(\Lambda/\sigma), \quad (10)$$

where the volume term,

$$f_{\mathrm{vol}}(\rho_{\mathrm{s}})=\rho_{\mathrm{s}}f_1(\rho_{\mathrm{s}}), \quad (11)$$

physically includes the free energy contributions from the integrated-out counterions and monomers of a single star. Stability with respect to spontaneous phase separation is guaranteed when $f_{\mathrm{fl}}(\rho_{\mathrm{s}})$ is convex, i.e.,

$$f_{\mathrm{fl}}''(\rho_{\mathrm{s}})>0, \quad (12)$$

where the primes denote differentiation with respect to the argument. Should there be phase coexistence between two states with densities $\rho_{\mathrm{s}}^{\mathrm{A}}$ and $\rho_{\mathrm{s}}^{\mathrm{B}}$, these are determined by the conditions of equality of pressures and chemical potentials, which read as

$$f_{\mathrm{fl}}(\rho_{\mathrm{s}}^{\mathrm{A}})-\rho_{\mathrm{s}}^{\mathrm{A}}f_{\mathrm{fl}}'(\rho_{\mathrm{s}}^{\mathrm{A}})=f_{\mathrm{fl}}(\rho_{\mathrm{s}}^{\mathrm{B}})-\rho_{\mathrm{s}}^{\mathrm{B}}f_{\mathrm{fl}}'(\rho_{\mathrm{s}}^{\mathrm{B}}), \quad (13)$$

$$f_{\mathrm{fl}}'(\rho_{\mathrm{s}}^{\mathrm{A}})=f_{\mathrm{fl}}'(\rho_{\mathrm{s}}^{\mathrm{B}}). \quad (14)$$

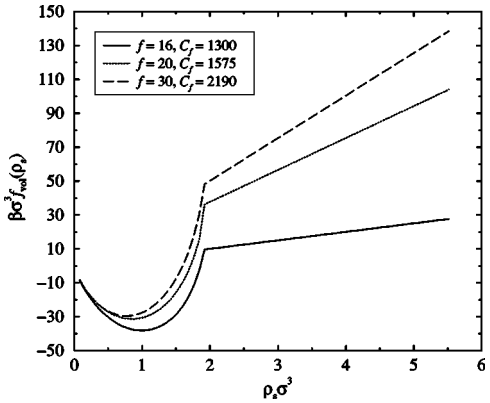

FIG. 2. The volume term $f_{\mathrm{vol}}(\rho_{\mathrm{s}})$ of PE star solutions as a function of the density ρ_{s} for three different functionalities f, as indicated in the legend, and for fixed charge ratio $\alpha=1/3$. For purposes of visualization, a thermodynamically irrelevant, linear term $C_f\rho_{\mathrm{s}}$ has been added to the volume terms, with the values of the constant C_f also being indicated in the legend.

Any terms in the free energy density that are linear in ρ_{s}, such as the last term in Eq. (10), have evidently no influence, neither on the stability criterion, Eq. (12), nor on the phase boundaries, Eqs. (13) and (14). Above the overlap concentration, $\rho_{\mathrm{s}}>\rho_{\mathrm{s}}^*$, $f_1(\rho_{\mathrm{s}})$ is a density independent constant, since there is no possibility for rearrangement of the counterions. Accordingly, $f_{\mathrm{vol}}(\rho_{\mathrm{s}})$ is just a linear function of the density that does affect the values of the chemical potential [see Eq. (14)] but has no influence on the phase behavior. A nontrivial density dependence of $f_{\mathrm{vol}}(\rho_{\mathrm{s}})$ occurs for $\rho_{\mathrm{s}}<\rho_{\mathrm{s}}^*$. As shown in Fig. 2, the volume term is a convex function of the density in this regime. This additional positive contribution to the second density derivative of the total free energy density is of crucial importance for the validity of the theory. Indeed, due to the fact that the effective interaction potential $V_{\mathrm{eff}}(D)$ softens with increasing density, the sum of the ideal and excess contributions to $f_{\mathrm{fl}}(\rho_{\mathrm{s}})$ turns out to be a concave function of ρ_{s} in the dilute regime $\rho_{\mathrm{s}}<\rho_{\mathrm{s}}^*$. If the volume term were ignored in this case, the apparent violation of Eq. (12) would imply there is an *unphysical* phase separation between two fluid phases. The volume term guarantees, therefore, the stability of the system against spontaneous liquid-gas coexistence.

Finally, we remark that the "cusp" of $f_{\mathrm{vol}}(\rho_{\mathrm{s}})$ at the overlap concentration ρ_{s}^*, which can be seen in Fig. 2, has its physical origin at a corresponding discontinuity of the first derivative of the number of free counterions as a function of the density. Indeed, as mentioned above, for $\rho_{\mathrm{s}}>\rho_{\mathrm{s}}^*$, N_3 vanishes identically, whereas for $\rho_{\mathrm{s}}<\rho_{\mathrm{s}}^*$ N_3 is a smooth function of ρ_{s}. Thus, N_3, which is the result of a minimization procedure, is not an analytic function of the density and shows at ρ_{s}^* a discontinuity in its first derivative, akin to that occurring for the order parameter in second-order

phase transitions. This nonanalyticity reflects itself in the discontinuity of the first derivative of the function $f_{\mathrm{vol}}(\rho_s)$ at the overlap density. It is nevertheless immaterial for the full thermodynamics of the system because it is compensated by a corresponding discontinuity of the opposite sign for the excess free energy term $f_{\mathrm{ex}}(\rho_s)$.

III. THE UNIFORM FLUID

In this section we use the above-derived effective Hamiltonian in order to calculate the pair structure as well as the free energy of uniform fluid phases of PE-star solutions. The structural data yield information on the correlations in the fluid, which show anomalies associated with the ultrasoft character of the pair interaction and with its peculiar density dependence. The free energy will be useful in drawing the phase diagram of the system.

A. Structure

As far as pair correlations are concerned, the basic quantity is the two-particle density operator $\hat{\rho}^{(2)}(\mathbf{r}_1,\mathbf{r}_2)$, defined through

$$\hat{\rho}^{(2)}(\mathbf{r}_1,\mathbf{r}_2;\{\mathbf{R}\})=\sum_{i\neq j}^{N_s}\delta(\mathbf{r}_1-\mathbf{R}_i)\delta(\mathbf{r}_2-\mathbf{R}_j). \tag{15}$$

The expectation value $\langle\hat{\rho}^{(2)}(\mathbf{r}_1,\mathbf{r}_2;\{\mathbf{R}\})\rangle$ of this operator is the two-particle density of the system, $\rho^{(2)}(\mathbf{r}_1,\mathbf{r}_2)$ which, for a translationally invariant fluid, depends only on $r\equiv|\mathbf{r}_1-\mathbf{r}_2|$. The radial distribution function (rdf), $g(r;\rho_s)$, is defined as

$$\rho^{(2)}(r)=\rho_s^2 g(r;\rho_s). \tag{16}$$

Introducing, moreover, the correlation function $h(r;\rho_s)$ as $h(r;\rho_s)=g(r;\rho_s)-1$, the structure factor $S(k;\rho_s)$ is defined as

$$S(k;\rho_s)=1+\rho_s\int d^3r\,\exp(-i\mathbf{k}\cdot\mathbf{r})h(r;\rho_s). \tag{17}$$

As is clear from Eqs. (8) and (9), the calculation of expectation values of quantities depending on the coordinates $\{\mathbf{R}\}$, such as the two-particle density operator in Eq. (15), involves the same standard rules that are valid for density independent interaction potentials. At a given, fixed density ρ_s, the latter acts simply as a parameter in the effective Hamiltonian that influences the form of the interaction. Hence, standard closure relations can be used to determine the pair structure of the fluid. In this work, we have employed the Rogers–Young closure[28] that interpolates between the Percus–Yevick and the hypernetted chain closures and contains an adjustable parameter ζ. For density independent potentials, ζ is fixed by the requirement of thermodynamic consistency between the compressibility and virial pressure routes to the free energy of the system. In the case at hand, where the interaction is density dependent, the virial route is not valid,[22–25] although the compressibility should be preserved if the correlation functions of the star centers remain invariant under the process of tracing out the monomers and the counterions.[29] However, the pair structure of our system at a given density ρ_s is *identical* to that of an imaginary fluid with a density-independent interaction which coincides with the potential $V_{\mathrm{eff}}(D;\rho_s)$. For this second fluid, enforcing the consistency of the compressibility and virial routes leads to a higher accuracy in the calculation of the pair structure. We follow, therefore, the procedure of enforcing consistency between the two routes, although none of them holds for the true system, with the single purpose of obtaining accurate pair correlations. The free energy of the system is subsequently calculated in an alternative way (see Sec. III B), which involve neither the pressure nor the compressibility routes.

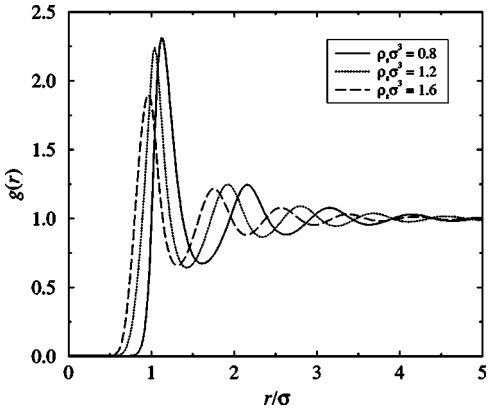

FIG. 3. The rdf $g(r)$ for PE-star solution for the arm number $f=15$ and charging fraction $\alpha=1/3$. The density decreases from the left to the right, but remains below the overlap concentration ρ_s^* in all cases.

In Fig. 3 we show the rdf $g(r)$ for three densities below the overlap value ρ_s^*. A striking feature is that, in contrast to usual fluids, the height of the main peak of $g(r)$ *decreases* with density, although its position moves towards smaller values of r. The second effect reflects the natural decrease in the nearest-neighbor distance within the fluid upon increase of the density. In atomic fluids, though, where the potential is steep and density independent, this is accompanied by a strengthening of the correlations. The opposite effect occurs here and it is a consequence of the fact that the effective potential $V_{\mathrm{eff}}(D;\rho_s)$ becomes *softer* as ρ_s grows, see Fig. 1.

Beyond the overlap density, an anomalous behavior of the fluid develops. This is first investigated by means of the rdf. In Fig. 4 we show the rdfs for a variety of densities $\rho_s>\rho_s^*$. As seen there, the position of the main peak of $g(r)$ ceases to decrease with growing density. Instead, a different development occurs: first a ''shoulder'' develops on the flank of the main peak of $g(r)$, as can be seen in Fig. 4 for $\rho_s\sigma^3=4.0$. Subsequently this shoulder grows into a new peak located at a distance smaller than the typical interparticle separation. In doing so, the height of the new peak steadily grows with increasing density, whereas the peak height of the main peak falls off. By further increasing the density the new peak surpasses the original main peak in height. This is characteristic for the anomalous fluid behavior, having its origin at the ultrasoft nature of the pair potential and being very similar to that seen for neutral star polymers.[30] The position of the second peak is not at twice the distance of the first peak, as occurs in the case of normal fluids. This is due to the fact that the position of the former is determined by the star

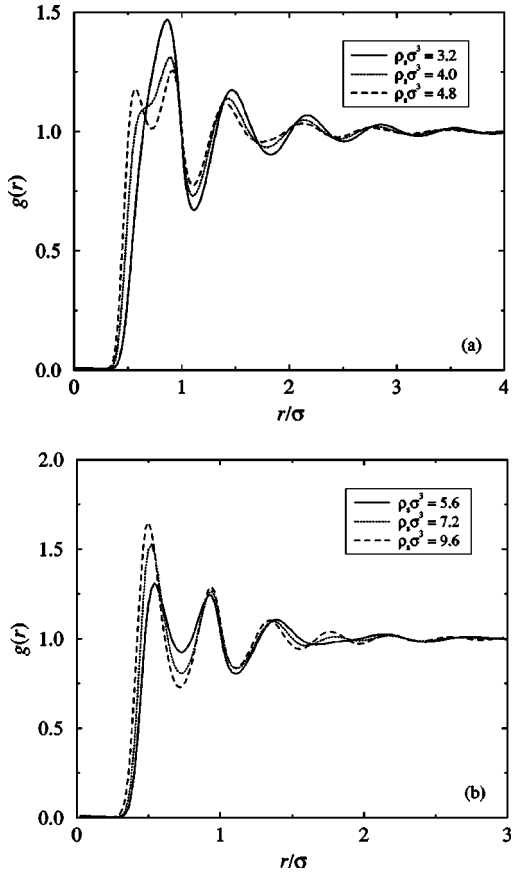

FIG. 4. The rdf $g(r)$ for a PE-star solution for $f=15$ and $\alpha=1/3$ for various densities exceeding the overlap value ρ_s^*.

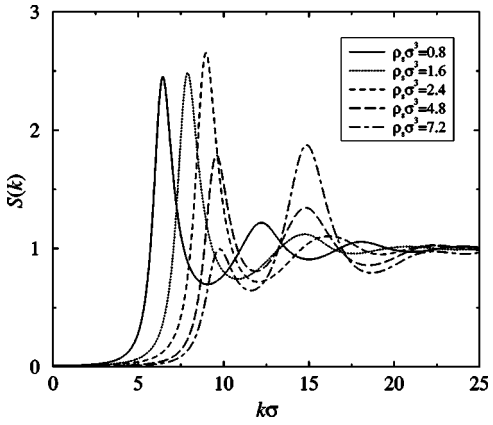

FIG. 5. The structure factor $S(k)$ for PE-star solution for $f=15$ and charging fraction $\alpha=1/3$ as function of the dimensionless wave vector $k\sigma$. The density grows from the left to the right.

diameter σ whereas the the position of the latter expresses a local clustering in the ultrasoft fluid. Each cluster is formed by particles at typical distances σ from a given, central one. The balance between the repulsions due to the neighbors outside the cluster and the soft repulsion from the internal ones determines the position of the first peak of $g(r)$, which is therefore not identical to the mean interparticle distance a. For densities above the overlap density it is energetically preferable to keep as many as possible particles outside of the star diameter of another particle. This helps reduce the energy of the whole system. Hence, the second peak of the rdf is located close to $r=\sigma$, where the potential is weak, since it has to vanish for $r>\sigma$.

The anomaly of $g(r)$ is reflected in the development and shape of the structure factor $S(k)$, as shown in Fig. 5. For densities far below the overlap density, the main peak shifts towards larger wave number for increasing density, as known for normal liquids. Close to the density $\rho_s^*\sigma^3=1.91$, the height of the main peak falls off, see Fig. 6(a). This is, once more, a reflection of the softening of the density dependent interaction potential $V_{\mathrm{eff}}(D;\rho_s)$ with increasing density.

For $\rho_s>\rho_s^*$, an anomalous evolution of $S(k)$ is observed, closely resembling the behavior seen for neutral star polymers. The height of the main peak decreases for increasing density and at the same time that of the second peak increases, surpassing the first one in height. This anomalous behavior of $S(k)$ can be explained by the two length scales present in the problem. On the one hand, there is the density dependent length scale $a\cong\rho_s^{-1/3}$, setting the typical interparticle distance in a normal fluid. On the other hand, we have a density-independent length scale, set by the star diameter σ, beyond which the interaction potential above the overlap density vanishes. For $\rho_s<\rho_s^*$, the particles move essentially within the Yukawa tails of the effective potential and they do not experience the ultrasoft core of the interaction. There, the pair correlations of the system are dominated by the length scale a. For $\rho_s>\rho_s^*$, both length scales play a role and the structure factor develops anomalies, see Fig. 6(b). Let us denote by k_n the position of the nth peak of the structure

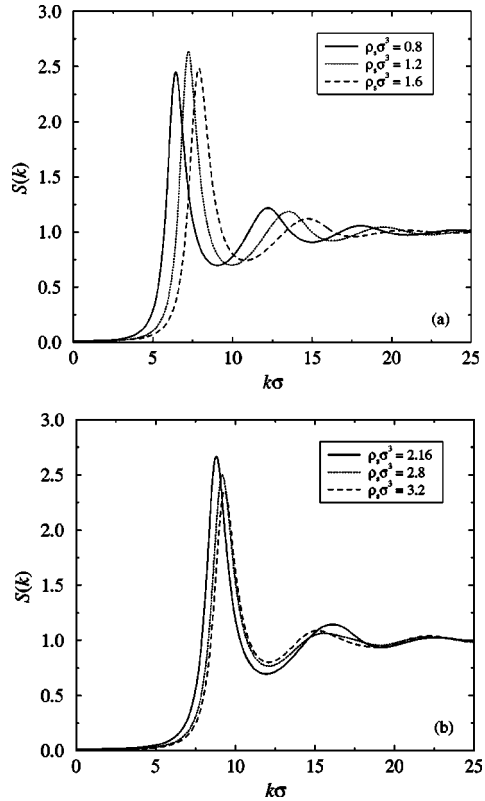

FIG. 6. The structure factor $S(k)$ of PE star solutions. (a) for densities below ρ^* and (b) for densities above ρ^*. As in Fig. 5, the parameters here are: $f=15$ and $\alpha=1/3$.

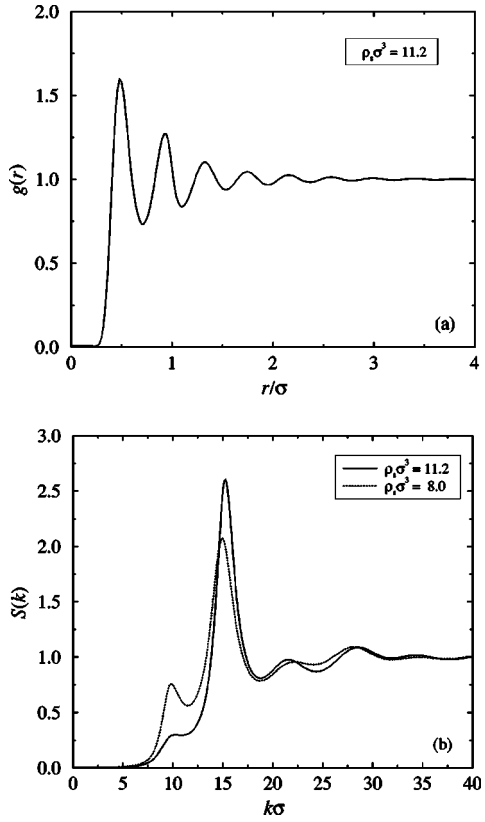

FIG. 7. (a) The rdf $g(r)$ and (b) the structure factor $S(k)$ obtained by the RY closure for $\rho_s\sigma^3=\rho_2=11.2$. In (b), the structure factor at $\rho_s\sigma^3=8.0$ is also plotted for comparison.

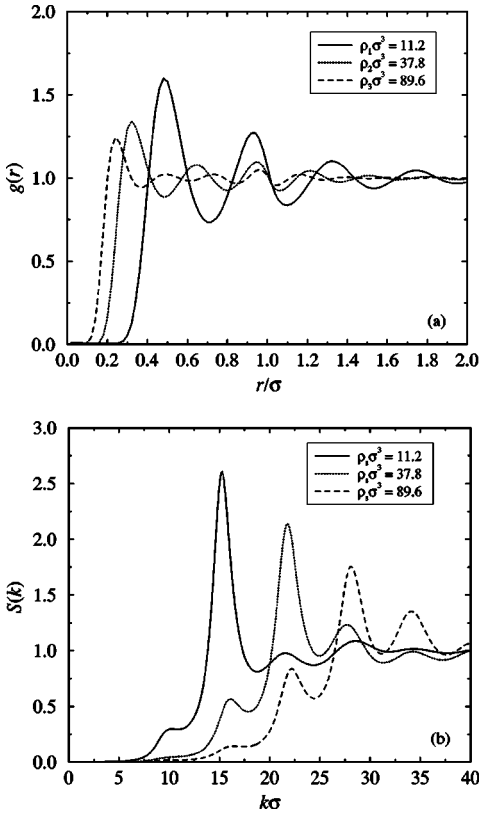

FIG. 8. (a) The radial distribution function $g(r)$ and (b) the structure factor $S(k)$ for the three magic density values ρ_m, $m=2,3,4$ defined in Eq. (18) of the text. The results refer to PE stars with $f=15$ arms and charging fraction $\alpha=1/3$.

factor. The position of the first peak of $S(k)$ is set by the length scale σ, i.e., $k_1\approx 2\pi/\sigma$. The length scale $\sigma-a$ sets the position of the second peak, i.e., $k_2\approx 2\pi/(\sigma-a)$. As demonstrated in Figs. 5 and 6(b), the position of the first peak remains nearly constant, whereas k_2 decreases with increasing density. This effect is due to the increase of the quantity $\sigma-a\approx\sigma-\rho_s^{-1/3}$ with ρ_s.

According to the above analysis, we can now surmise that the first peak of the structure factor disappears altogether if we tune the density in such a way that the two length scales, a and $\sigma-a$ roughly coincide, i.e., $\sigma=2a$. This should occur when $g(r)$ shows exactly two oscillations of wavelength a between $r=0$ and $r=\sigma$. In Fig. 7(a) we show the rdf for $\rho_s\sigma^3=11.2$, which shows precisely two oscillations[31] in the interval $[0,\sigma]$. We call this density ''magic'' density ρ_2, where the index labels the number of oscillations between 0 and σ. Concomitantly, the structure factor has an extremely high peak for this density value, which is located at the position $2\pi/a\approx 4\pi/\sigma$. In Fig. 7(b), we show $S(k)$ at $\rho_s=\rho_2$, together with $S(k)$ at density for $\rho_s\sigma^3=8$, in order to illustrate the disappearance and replacement of the first peak through the second one. The anomaly of $S(k)$ is twofold. On the one hand, the successive peaks are not located at positions that are integer multiples of one another. On the other hand, the heights of the peaks evolve in a peculiar way, a peak appearing as the highest in a certain range of densities, then losing in height in order to be replaced by the next one as the highest, and so on.

It is challenging to investigate what happens if the density is further increased. Does the new main peak increase further indicating a freezing of the whole system, or does the scenario observed for the first peak repeat? We have solved the RY closure up to the density $\rho_s=90$, finding out the the second possibility materializes. The height of the main peak falls off and the originally third peak becomes the highest one by further increasing the density, as demonstrated in Fig. 8(b). This behavior can be attributed to development of more and more oscillations of $g(r)$ in the interval $[0,\sigma]$, see Fig. 8(a). One can repeat the argument for the magic density ρ_2: the structure factor $S(k)$ will be dominated by a single length scale if there is an integer number m of oscillations in $g(r)$ within the interval $[0;\sigma]$. This occurs for a sequence of magic densities ρ_m, the index denoting the number of the aforementioned oscillations. Knowing the magic density ρ_2, it is an easy exercise to show that the ρ_m is related to ρ_2 through

$$\rho_m=\left(\frac{m}{2}\right)^3\rho_2, \quad m=3,4,5,\ldots . \tag{18}$$

Using $\rho_2\sigma^3=11.2$ we obtain $\rho_3\sigma^3=37.8$ and $\rho_4\sigma^3=89.6$.

The above results can be nicely summarized in a double logarithmic plot. In Fig. 9 we show the first few peak positions of $S(k)$ as function of the density; we stress that when we talk about the nth peak we actually mean the peak which is the nth peak at lower densities, where the system behaves as a normal fluid. The reason is the disappearance and replacement of the ''first'' peaks through peaks of higher or-

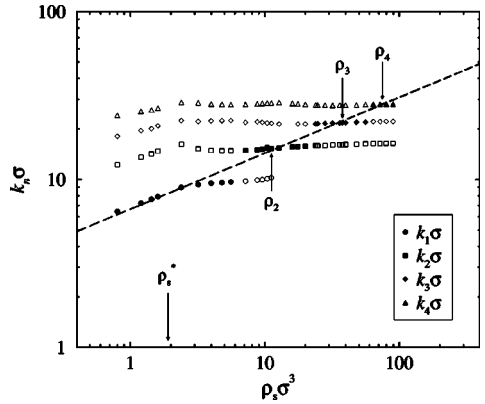

FIG. 9. Double logarithmic plot showing the position of the maxima of $S(k)$ as a function of the density $\rho_s\sigma^3$. The filled symbols denote the highest peak. The arrows on the plot indicate the positions of the magic densities ρ_m, whereas the arrow on the horizontal axis denotes the overlap density ρ_s^*. The dashed line has slope 1/3.

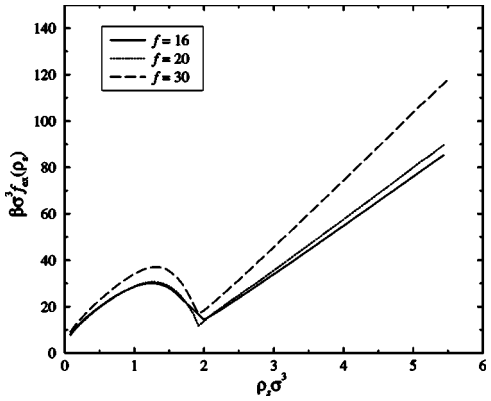

FIG. 10. The excess free energy density $f_{ex}(\rho_s)$ of a fluid of PE stars as a function of the concentration ρ_s. The results have been obtained through the λ-integration route described in the text and pertain to stars with $\alpha=1/3$.

ders. Thus, the maximum of first order becomes the one of second order and so on. The filled symbols in Fig. 9 denote the highest peak. From this figure, we can draw the following conclusions: the fluid that interacts by the ultrasoft, density-dependent potential is normal for all densities $\rho_s \lesssim \rho_s^*$. In this regime, the position of the first maximum scales with the density as $k_1 \sim \rho_s^{1/3}$. The maxima of higher order are located at positions $k_n = nk_1$, meaning that only one length scale determines the structure of the system. Above overlap, this is not true anymore; the positions of the maxima become very insensitive to changes in the density, in agreement with the experimental observations of Heinrich *et al.*[19] However, if we extrapolate the line with slope 1/3 to higher densities, we find that this line passes through the magic densities ρ_m of Eq. (18). At these density values, the two competing length scales of the problem become integer multiples of one another, yielding again the usual scaling behavior of the position of the main peak with the density, $k_{max} \sim \rho_s^{1/3}$.

B. Thermodynamics

With the ideal term $f_{id}(\rho_s)$ and the volume contribution $f_{vol}(\rho_s)$ to the free energy density of the fluid already determined [see Eq. (10)], we need now to calculate the excess contribution, $f_{ex}(\rho_s)$ in order to access the full thermodynamics of the system. As the density dependence of the interaction rules out the application of the compressibility and virial pressure routes (32) we resort to a different technique that is valid for the interaction potential at hand. From Eqs. (8) and (15), it follows that the interaction part of the Hamiltonian can be expressed as

$$\sum_{i\neq j}^{N_s} V_{eff}(|\mathbf{R}_i - \mathbf{R}_j|;\rho_s) = \int d^3r_1 \int d^3r_2 \hat{\rho}^{(2)}(\mathbf{r}_1,\mathbf{r}_2;\{\mathbf{R}\}) V_{eff}(|\mathbf{r}_1-\mathbf{r}_2|;\rho_s). \quad (19)$$

Regarding now the excess free energy as a functional of the interaction potential, $F_{ex} = F_{ex}[V_{eff}]$, introducing Eq. (19) above into Eq. (6) and making use of Eq. (7), we find that irrespective of the explicit density dependence of the interaction, it holds[33]

$$\frac{\delta F_{ex}[V_{eff}]}{\delta V_{eff}(\mathbf{r}_1,\mathbf{r}_2;\rho_s)} = \frac{1}{2}\rho^{(2)}(|\mathbf{r}_1-\mathbf{r}_2|) = \frac{1}{2}\rho_s^2 g(r;\rho_s). \quad (20)$$

The last equation provides the so-called λ-*integration route* to the excess free energy of the system.[33] We introduce a linear path of 'charging' the effective potential that depends on a parameter λ and reads as

$$V_{eff}^{(\lambda)}(\mathbf{r}_1,\mathbf{r}_2;\rho_s) = \lambda V_{eff}(\mathbf{r}_1,\mathbf{r}_2;\rho_s), \quad (21)$$

such that for $\lambda=0$ we obtain an ideal system and for $\lambda=1$ the full interacting system. Along this path, Eq. (20) can be integrated to yield[25]

$$f_{ex}(\rho_s) = \frac{1}{2}\rho_s^2 \int d^3r V_{eff}(r;\rho_s) \int_0^1 d\lambda g^{(\lambda)}(r;\rho_s), \quad (22)$$

with $g^{(\lambda)}(r;\rho_s)$ being the radial distribution function corresponding to the potential $\lambda V_{eff}(r;\rho_s)$ instead of $V_{eff}(r;\rho_s)$. For $\lambda=0$, it is $g^{(0)}(r;\rho)=1$, i.e., we have the rdf for a homogeneous, noninteracting fluid. For $\lambda=1$, it holds $g^{(1)}(r;\rho_s) = g(r;\rho_s)$, i.e., we have the rdf of the real system.

We have thus employed Eq. (22) to calculate the excess part of the free energy. For every density ρ_s, we have calculated the family of radial distribution functions $g^{(\lambda)}(r;\rho)$ by solving the Rogers–Young integral equation, as discussed in Sec. III. In Fig. 10, we show the resulting excess free energy density $f_{ex}(\rho_s)$ for charge fraction $\alpha=1/3$. A discussion regarding the validity of the compressibility sum rule and a comparison between the λ-integration result and the structural prediction for the isothermal compressibility of the system are shown in the Appendix. Due to the softening of the effective potential with increasing density below the overlap concentration, the excess free energy density shows a nonconvex behavior for $\rho_s < \rho_s^*$. Were $f_{ex}(\rho_s)$ to be the only contribution to the free energy density of the fluid, this concavity would signal spontaneous phase separation into a gas and a liquid. However, when the ideal and volume terms are added to the excess contribution, a convex free energy results, as shown in Fig. 11. Thus, we see that the volume term

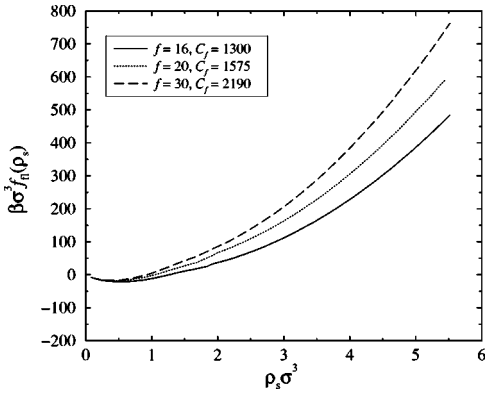

FIG. 11. The total free energy density $f_{\rm fl}(\rho_{\rm s})=f_{\rm id}(\rho_{\rm s})+f_{\rm ex}(\rho_{\rm s})+f_{\rm vol}(\rho_{\rm s})$ for a PE-star fluid with the same parameters as in Fig. 10. Note that the concave part and the cusp of the excess free energy contribution are eliminated by the convexity and the corresponding cusp of the volume term shown in Fig. 2, to produce a smooth curve that is concave-up. For clarity, linear terms of the form $C_f\rho_{\rm s}$ have been added to the results, with the values of the constants C_f being denoted in the legend.

here has the effect of *stabilizing* the fluid against phase separation, a feature *opposite* to that observed for charge-stabilized colloidal suspensions in the presence of salt.[34] These differences quite probably arise from the fact that we are dealing here with penetrable objects rather than with hard colloids, and also due to the fact that the instability predicted in Ref. 34 occurs for nonvanishing salt concentration, whereas we examine a salt-free system here.

IV. CRYSTALLINE PHASES

Having calculated the free energy of the homogeneous, fluid phase, we turn in this section our attention to that of various candidate crystalline phases, so as to be able to draw the phase diagram of the system in what will follow. For the crystalline solids, we employ the approximate Einstein model.[35,36] The latter is based on the Gibbs–Bogoliubov inequality, which relates the Helmholtz free energy F of a given system described by the (effective) Hamiltonian $\mathcal{H}_{\rm eff}$, to the Helmholtz free energy F_0 of a reference system with Hamiltonian $\mathcal{H}_0$, as

$$F\leqslant\tilde{F}\equiv F_0+\langle\mathcal{H}_{\rm eff}-\mathcal{H}_0\rangle_0=F_0+\langle U_{\rm eff}-U_0\rangle_0. \tag{23}$$

Here, $U_{\rm eff}$ and U_0 stand for the potential energy functions of the effective and the reference Hamiltonians, respectively, and the $\langle\ldots\rangle_0$ symbol denotes a canonical average performed with the Hamiltonian of the reference system. This procedure is useful if (a) a Hamiltonian $\mathcal{H}_0$ can be found that is close to that of the real system in the prescribed ordered state; (b) $\mathcal{H}_0$ allows for a straightforward calculation of F_0 and $\langle\mathcal{H}-\mathcal{H}_0\rangle_0$ and (c) the reference Hamiltonian $\mathcal{H}_0$ contains at least one variational parameter to minimize the right-hand side of the inequality (23). As this method only provides an upper bound for the Helmholtz free energy, the presence of the variational parameter(s) in $\mathcal{H}_0$ is important in optimizing that upper bound.

Since we are dealing with a soft interaction between PE stars, the potential energy felt by each particle in the ordered lattice can be locally approximated by a quadratic function of its deviation from its equilibrium position. Hence, a harmonic approximation is justified and we choose as reference Hamiltonian that of the Einstein model. In this model, the particles are noninteracting but are bounded to the equilibrium lattice positions by harmonic springs of spring constant ξ. Thus, $\mathcal{H}_0$ reads as

$$\mathcal{H}_0=\sum_{i=1}^{N}\left[\frac{\mathbf{P}_i^2}{2m}+\frac{\xi}{2}(\mathbf{R}_i-\mathbf{S}_i)^2\right], \tag{24}$$

where the set $\{\mathbf{S}_i\}$ spans the prescribed lattice. Let also $\{\mathbf{K}_i\}$ be the set of reciprocal lattice vectors (RCVs) of the lattice. In what follows, the spring constant ξ plays the role of a variational parameter and, for noncubic lattices, the size ratios in the conventional unit cell will be used as additional ones. Since the kinetic energies in the reference and the real Hamiltonians coincide, we are left to calculate the potential energy of both systems.

The calculation of the Helmholtz free energy of the harmonic solid easily yields

$$\frac{F_0}{N}=\frac{3}{2}k_BT\ln\left(\frac{\tilde{\alpha}}{\pi}\right)+3k_BT\ln\left(\frac{\Lambda}{\sigma}\right), \tag{25}$$

where

$$\tilde{\alpha}=\frac{\beta\xi\sigma^2}{2}. \tag{26}$$

Equally, the calculation of the canonical average of the potential energy U_0 is straightforward and we obtain

$$\frac{\langle U_0\rangle_0}{N}=\frac{3}{2}k_BT. \tag{27}$$

The calculation of $\langle U_{\rm eff}\rangle_0$ is more involved, but it can nevertheless be reduced to that of one-dimensional integrals as

$$\frac{\langle U_{\rm eff}\rangle_0}{N}=\frac{1}{2}\sum_{j\neq0}n_j\left(\frac{\tilde{\alpha}}{2\pi}\right)^{1/2}\frac{1}{X_j}\int_0^\infty dx V_{\rm eff}(x;\rho_{\rm s})x \times\{\exp[-\tilde{\alpha}(x-X_j)^2/2]-\exp[-\tilde{\alpha}(x+X_j)^2/2]\}. \tag{28}$$

The sum on the right-hand side counts all shells of lattice vectors with the exception of $j=0$ (self-interaction). The quantity n_j denotes the number of equal lattice vectors belonging to the same shell; $X_j=|\mathbf{S}_j|/\sigma$ are dimensionless lattice vectors and, accordingly, $x=D/\sigma$. For $T=0$, i.e., in the limit $\tilde{\alpha}\to\infty$, Eq. (28) reduces to the expression for the lattice sum

$$\frac{\langle U_{\rm eff}\rangle_0}{N}=\frac{1}{2}\sum_{j\neq0}n_jV_{\rm eff}(X_j). \tag{29}$$

For computation purposes, an alternative expression to Eq. (28) is useful. It involves the Fourier transform $\tilde{V}_{\rm eff}(k;\rho_{\rm s})$ of the effective interaction at wave number k and reads as

$$\frac{\langle U_{\mathrm{eff}}\rangle_0}{N} = \frac{\sigma^3}{2v_c}\sum_{\{\mathbf{Q}\}} \exp[-Q^2/(2\tilde{\alpha})]\tilde{V}_{\mathrm{eff}}(Q;\rho_s) - \frac{1}{4\pi^2}\int_0^\infty dq\, q^2 \exp[-q^2/(2\tilde{\alpha})]\tilde{V}_{\mathrm{eff}}(q;\rho_s), \tag{30}$$

where v_c denotes the volume of the primitive cell of the corresponding lattice in direct space, $q=k\sigma$ and $\{\mathbf{Q}\}$ is the set of all dimensionless reciprocal lattice vectors, $\mathbf{Q}_i=\mathbf{K}_i\sigma$. Equations (28) and (30) are completely equivalent; for weak localization of the particles around the lattice sites (small $\tilde{\alpha}$), Eq. (30) is more suitable, since a summation over a few reciprocal-lattice shells suffices to guarantee convergence of the sum, whereas for strong localization (large $\tilde{\alpha}$), Eq. (28) is computationally more convenient.

We tried a large number of candidate crystal structures with various symmetries and minimized the free energy $\tilde{F}$ of Eq. (23) with respect to all variational parameters available. The lattices we considered were the simple cubic (sc), the body-centered-cubic (bcc), the face-centered-cubic (fcc), the body-centered orthogonal (bco), as well as the hexagonal-close-packed (hcp) structure, the simple hexagonal (hex), the trigonal,[37] the diamond, and the A15 lattices.[38–40] These augment considerably the set used previously in carrying out lattice sum ($\tilde{\alpha}\to\infty$) calculations.[21]

With F_{min} denoting the value of the variational free energy $\tilde{F}$ at the minimum with respect to the variational parameters, the total free energy of the crystal, $F_{\mathrm{sol}}(\rho_s)$ is finally obtained by adding to F_{min} the state-independent volume term $F_{\mathrm{vol}}(\rho_s)$. The winning phase at fixed density is the one with the lowest value of $F_{\mathrm{sol}}(\rho_s)$. Finally, the free energy density $f_{\mathrm{sol}}(\rho_s)$ is obtained as $F_{\mathrm{sol}}(\rho_s)/\Omega$.

V. THE PHASE DIAGRAM

With the free energy densities of all phases, fluid, and solid being available, the phase diagram can be drawn by performing the common tangent construction on the $f_{\mathrm{fl}}(\rho_s)$ curves and $f_{\mathrm{sol}}(\rho_s)$ curves.[41] A preliminary phase diagram for the system at hand has been drawn in Ref. 21. There, the stable crystalline phases were determined on the basis of lattice sum calculations only; no minimization of the free energy was carried out. Moreover, the phase boundary with the fluid phase has been determined on the basis of the Hansen–Verlet criterion,[42] which states that the fluid crystallizes when the main peak of the structure factor attains the value 2.85. The present calculation is more accurate, in the sense that it is based on the free energies of the various phases. A comparison with the rough phase diagram derived before,[21] allows us also to test the reliability of the Hansen-Verlet freezing criterion. Although the latter has been proven to be rather accurate for systems interacting with ''hard'' interactions, it has been shown to lose its validity for the high-density crystals of ultrasoft systems, such as ionic microgels.[37]

We have kept the charging fraction fixed at $\alpha=1/3$ varying the functionality and the density. The resulting phase diagram is shown in Fig. 12. The solid phases have nearly

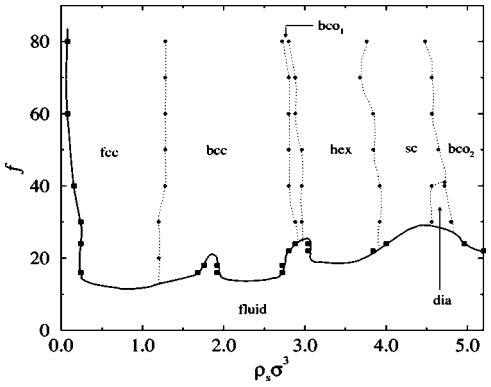

FIG. 12. Phase diagram for PE stars for fixed charging fraction $\alpha=1/3$. The points denotes the phase transition between different crystal structures, the squares denote the fluid–solid transition. The density gaps between the coexisting phases are extremely small, hence they are not shown in the figure. The lines are guides to the eye.

the same sequence as in the phase diagram obtained by lattice sum calculations.[21] For small densities, the fcc lattice is favored followed by the bcc lattice for increasing density. Further increasing the density, a body-centered orthogonal phase appears, which we call bco_1 lattice, to differentiate it from another one that is stable at higher densities. The size ratios for this bco_1 lattice are 1:0.5:0.5, i.e., the crystal has two equal small edges and one large edge for its conventional unit cell. Due to the equality of the two edges, this is then a *body-centered tetragonal* (bct) lattice, with a higher degree of symmetry than the general bco. In contrast to the preliminary phase diagram,[21] a simple hexagonal lattice shows up for densities $\rho_s\sigma^3\gtrsim 3.0$. For higher densities the sc, diamond, and, an additional, bco_2 lattice turn out to be stable. The size ratios for the bco_2 crystal are 1:1:0.5 (two large edges and one small), and we have again a bct lattice. The size ratios for both the bco_1 and the bco_2 crystals equal exactly the ones obtained by lattice sum calculations, i.e., the effects of the finite temperature on the geometry of the crystal are negligible, an effect also seen in the case of neutral star polymers.[43] In summarizing, we can say that the lattice sum calculation have yielded the same sequence of lattice types below the overlap concentration, however, new crystal phases turn out to be stable above the overlap density, where the ultrasoft part of the interaction potential becomes relevant. Alternatively, the Hansen-Verlet criterion is valid when the particles feel the Yukawa part of the effective interaction but it breaks down for higher densities. This finding is in line with recent results on the phase behavior of ionic microgels.[37] The ultrasoft interaction is responsible for stabilizing a number of exotic phases, including a small domain of stability of the diamond lattice. The occurrence of unusual crystal structures for systems interacting by means of ultrasoft potentials has been explicitly confirmed in star polymers[40,43] and microgels.[37] Some general physical and geometrical arguments supporting the stability of such phases have been put forward recently by Ziherl and Kamien.[38,39]

The system remains always fluid for small arm numbers or/and small densities. Switching to larger functionalities, we observe a sequence of several reentrant melting transitions

keeping the arm number fixed at about $f \approx 15$. We found no stable crystal phases for $f = 10$, thus the 'critical functionality' f_c below which no freezing is possible lies in our case in the interval $10 < f_c < 15$. Note that, for neutral star polymers,[43] this quantity has the value $f_c = 34$. The fact that charged stars crystallize more easily than neutral ones has been already conjectured in Ref. 8 and reflects the fact that the effective repulsion of charged stars is stronger than that of neutral ones at a given dimensionless density $\rho_s \sigma^3$. Finally, we remark that we anticipate that the phase diagram of Fig. 12 will maintain its topology also for different charging fractions α. The main difference will be an expansion of the domain of stability of the fluid phase for decreasing α, since in this case the effective interaction becomes less repulsive.

VI. CONCLUSIONS

We have presented calculations on the structural and thermodynamic properties of osmotic polyelectrolyte stars, based on a coarse-grained description that employs effective interactions between the star centers. The anomalous structure that characterizes concentrated PE-star solutions has its physical origins at the ultrasoft character of the effective interaction potential and also at its particular density dependence. In principle, the findings of our work should be verifiable in scattering experiments in which only the centers of the stars are visible and scattering from the chains and the counterions is suppressed. Our theory provides indeed an explanation for the anomalous behavior of the main peak position of the interstar structure factor reported in Ref. 19. Certainly, more work is desirable on the experimental side in deriving reliable structure factors that can be compared with the theoretical ones in a wide range of wave vectors and concentrations.

The theoretical predictions for the richness of the phase diagram and the occurrence of various crystalline phases can also be experimentally tested, whereby the synthesis of PE stars with a high degree of monodispersity is very important, since polydispersity can destroy crystalline order. In principle, our effective potential can also be employed in a study of the glass transition of the PE solution, in full analogy with the case of neutral star polymers.[44] The explicit density dependence of the pair potential and the irrelevance of the volume terms in calculating the ergodic-to-nonergodic transition within the framework of mode-coupling theory may lead in this case to an unexpected behavior of the vitrification line of the system at hand. Finally, we comment that although we have neglected the ubiquitous many-body forces between PE stars and based our analysis exclusively on pair potentials, our calculations show[45] that three-body forces become appreciable only at concentrations exceeding ρ_s^* by a factor 3–4, hence we expect all predictions presented in this work to maintain their validity also in the presence of many-body terms in the interaction potential.

ACKNOWLEDGMENTS

The authors thank Arben Jusufi and Dieter Gottwald for helpful discussions. This work was supported by the Deutsche Forschungsgemeinschaft (DFG), within the Transregio-Sonderforschungsbereich SFB-TR6, "Physics of Colloidal Dispersions in External Fields," Subproject C3.

APPENDIX: ON THE CONSISTENCY BETWEEN THE λ-INTEGRATION AND THE COMPRESSIBILITY ROUTES TO THE FREE ENERGY

In this Appendix we briefly discuss the question of the consistency between the compressibility obtained from the low-k-limit of the structure factor and that derived by differentiating the free energy obtained through the λ-integration route described in Sec. III B. Consider a multicomponent mixture, in which all but one remaining component (labeled '1') have been traced out, so that one ends with an effective description of the remaining one-component system via an effective Hamiltonian $\mathcal{H}_{\text{eff}}$. If the integration of all other degrees of freedom is carried out exactly, then the pair correlation functions $g_{11}(r)$ and $S_{11}(k)$ remain invariant under the cross over to an effective description.[20,29] For mixtures of neutral species, in which the particle number for each component can fluctuate independently of that for the other, the *partial* osmotic compressibility of species 1, $\chi_T^{(1)}$ is given by

$$\rho_1 k_B T \chi_T^{(1)} = S_{11}(k=0), \tag{A1}$$

whereas in order to obtain the *total* compressibility of the multicomponent mixture, additional information about the dependence of the osmotic pressure on the activities of the integrated components is necessary.[29] On the other hand, if one deals with a two-component, salt-free, electroneutral mixture of charged spheres, the total compressibility χ_T is indeed obtainable via $S_{11}(k)$ alone, since the long-range nature of the Coulomb interaction, the electroneutrality and the perfect-screening conditions, lead to the result[46]

$$\rho_s k_B T \chi_T = S_{11}(k=0), \tag{A2}$$

where we have used the symbol ρ_s for the number density of species 1 (the star centers).

At the same time, from the thermodynamic definition of the compressibility, we obtain

$$\rho_s k_B T \chi_T = \frac{1}{\rho_s \beta f''(\rho_s)}, \tag{A3}$$

with the free energy density $f(\rho_s)$ and the primes denoting differentiation with respect to the argument. We have tested the consistency between structure and λ-integration route by calculating the quantity $\rho_s k_B T \chi_T$ directly from Eq. (A2) using Rogers-Young structural data and from Eq. (A3) by taking the second derivative of the free energy obtained from the λ-integration route. The comparison is shown in Fig. 13. It can be seen that the two are in fairly good agreement with one another throughout the broad concentration range and only at very small densities do considerable deviations appear. The discrepancies are most likely due to inaccuracies in the derivation of the effective interaction potential. Discrepancies between the two routes could also arise from the approximate nature of the Rogers-Young closure used to calculate structural data, however, this closure has been shown to

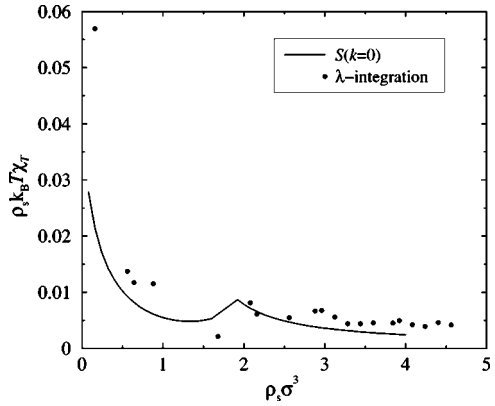

FIG. 13. Comparison between the 'structural' [solid line, Eq. (A2)] and the 'λ-route' [points, Eq. (A3)] total compressibilities of a PE star solution. The results shown here are for PE stars of functionality $f=20$ and charge fraction $\alpha=1/3$.

be very accurate for purely repulsive interactions. Hence, we tend to believe that it is rather the approximate character of the pair potential that leads to the difference between the compressibility and λ-integration routes. Notice that the 'noisy' result for the λ integration is a consequence of taking a second derivative numerically.

[1] J. Klein Wolterink, J. van Male, M. A. Cohen Stuart, L. K. Koopal, E. B. Zhulina, and O. V. Borisov, Macromolecules **35**, 9176 (2002).
[2] P. Pincus, Macromolecules **24**, 2912 (1991).
[3] J. Klein Wolterink, F. A. M. Leermakers, G. J. Fleer, L. K. Koopal, E. B. Zhulina, and O. V. Borisov, Macromolecules **32**, 2365 (1999).
[4] O. V. Borisov and E. B. Zhulina, J. Phys. II **7**, 449 (1997).
[5] O. V. Borisov and E. B. Zhulina, Eur. Phys. J. B **4**, 205 (1998).
[6] N. P. Shusharina, P. Linse, and A. R. Khokhlov, Macromolecules **33**, 3892 (2000).
[7] A. Jusufi, C. N. Likos, and H. Löwen, Phys. Rev. Lett. **88**, 018301 (2002).
[8] A. Jusufi, C. N. Likos, and H. Löwen, J. Chem. Phys. **116**, 11011 (2002).
[9] M. Roger, P. Guenoun, F. Muller, L. Belloni, and M. Delsanti, Eur. Phys. J. E **9**, 313 (2002).
[10] O. V. Borisov and E. B. Zhulina, Macromolecules **35**, 4472 (2002).
[11] E. B. Zhulina and O. V. Borisov, Macromolecules **35**, 9191 (2002).
[12] O. V. Borisov and E. B. Zhulina, Macromolecules **36**, 10029 (2003).
[13] P. Guenoun, F. Muller, M. Delsanti, L. Auvray, Y. J. Chen, J. W. Mays, and M. Tirrell, Phys. Rev. Lett. **81**, 3872 (1998).
[14] W. Groenewegen, S. U. Egelhaaf, A. Lapp, and J. R. C. van der Maarel, Macromolecules **33**, 3283 (2000).
[15] W. Groenewegen, A. Lapp, S. U. Egelhaaf, and J. R. C. van der Maarel, Macromolecules **33**, 4080 (2000).
[16] J. R. C. van der Maarel, W. Groenewegen, S. U. Egelhaaf, and A. Lapp, Langmuir **16**, 7510 (2000).
[17] X. Guo and M. Ballauff, Phys. Rev. E **64**, 051406 (2001).
[18] N. Dingenouts, R. Merkle, X. Guo, T. Narayan, G. Goerick, and M. Ballauff, J. Appl. Crystallogr. **36**, 578 (2003).
[19] M. Heinrich, M. Rawiso, J. G. Zilliox, P. Lesieur, and J. P. Simon, Eur. Phys. J. E **4**, 131 (2001).
[20] C. N. Likos, Phys. Rep. **348**, 267 (2001).
[21] C. N. Likos, N. Hoffmann, A. Jusufi, and H. Löwen, J. Phys.: Condens. Matter **15**, S233 (2002).
[22] A. A. Louis, J. Phys.: Condens. Matter **14**, 9187 (2002).
[23] F. H. Stillinger, H. Sakai, and S. Torquatto, J. Chem. Phys. **117**, 288 (2002).
[24] H. Sakai, F. H. Stillinger, and S. Torquatto, J. Chem. Phys. **117**, 297 (2002).
[25] C. F. Tejero and M. Baus, J. Chem. Phys. **118**, 892 (2003).
[26] J. A. Barker, D. Henderson, and W. R. Smith, Mol. Phys. **17**, 579 (1969).
[27] The importance of such terms has been first discussed in J. S. Rowlinson, Mol. Phys. **52**, 567 (1984). A derivation of the volume term for the case of liquid metals, which include a quantal component (the free electrons), has been given in N. W. Ashcroft and D. Stroud, Solid State Phys. **33**, 1 (1987). For a discussion of the influence of the volume term on the phase behavior of typical soft matter systems, such as polymers and charged colloids, see Ref. 20.
[28] F. J. Rogers and D. A. Young, Phys. Rev. A **30**, 999 (1984).
[29] M. Dijkstra, R. van Roij, and R. Evans, J. Chem. Phys. **113**, 4799 (2000).
[30] M. Watzlawek, H. Löwen, and C. N. Likos, J. Phys.: Condens. Matter **10**, 8189 (1998).
[31] Taking $\sigma=2a$ and $a=\rho_s^{-1/3}$ one would obtain the value $\rho_s\sigma^3=8$ instead. However, the relation between a and ρ_s involves some proportionality factor of order unity and hence the value $\rho_s\sigma^3=11.2$ results.
[32] J.-P. Hansen and I. R. McDonald, *Theory of Simple Liquids*, 2nd ed. (Academic, New York, 1986).
[33] R. Evans, Adv. Phys. **28**, 143 (1979).
[34] R. van Roij, M. Dijkstra, and J.-P. Hansen, Phys. Rev. E **59**, 2010 (1999).
[35] N. W. Ashcroft and N. D. Mermin, *Solid State Physics* (Holt Saunders, Philadelphia, 1976).
[36] C. F. Tejero, A. Daanoun, H. N. W. Lekkerker, and M. Baus, Phys. Rev. E **51**, 558 (1995).
[37] D. Gottwald, C. N. Likos, G. Kahl, and H. Löwen, Phys. Rev. Lett. **92**, 068301 (2004).
[38] P. Ziherl and R. D. Kamien, Phys. Rev. Lett. **85**, 3528 (2000).
[39] P. Ziherl and R. D. Kamien, J. Phys. Chem. B **105**, 10147 (2001).
[40] C. N. Likos, N. Hoffmann, H. Löwen, and A. A. Louis, J. Phys.: Condens. Matter **14**, 7681 (2002).
[41] The common tangent construction amounts to solving Eqs. (13) and (14) with f_{fl} being replaced by f_{sol} on one side of the equations if we are interested in the freezing transition or on both sides if we want to determine phase boundaries between crystals of different symmetries.
[42] J.-P. Hansen and L. Verlet, Phys. Rev. **184**, 151 (1969).
[43] M. Watzlawek, C. N. Likos, and H. Löwen, Phys. Rev. Lett. **82**, 5289 (1999).
[44] G. Foffi, F. Sciortino, P. Tartaglia, E. Zaccarelli, F. Lo Verso, L. Reatto, K. Dawson, and C. N. Likos, Phys. Rev. Lett. **90**, 238301 (2003).
[45] C. N. Likos (unpublished).
[46] See, e.g., Sec. 10.2 of Ref. 32. Note that due to a different definition of the structure factors in Ref. 32, a division by the concentration x_1 of species 1 appears in the right-hand side of the compressibility equation. This stems from the fact that the partial structure $S_{11}(k)$ tends to x_1 for $k\to\infty$, i.e., it differs from the structure factors used in this paper by a factor x_1.